京都大学数理解析研究所 RIMS共同研究「非線形波動現象の数理とその応用」, October 17, 2019

非定常波形解析による波浪中抵抗増加に関する流体力学的研究

Hydrodynamic Study on Added Resistance by Means of Unsteady Wave Analysis

Masashi Kashiwagi
Department of Naval Architecture & Ocean Engineering, Osaka University
2-1 Yamada-oka, Suita, Osaka 565-0871, Japan

1. Abstract

It is known that the added resistance in waves can be computed from ship-generated unsteady waves through the unsteady wave-analysis method. In order to investigate the effects of nonlinear ship-generated unsteady waves and bluntness of the ship geometry on the added resistance, measurements of unsteady waves, wave-induced ship motions and added resistance are carried out using two different (blunt and slender) modified Wigley models. The ship-generated unsteady waves are also produced by the linear superposition using the waves measured for the diffraction and radiation problems and the complex amplitudes of ship motions measured for the motion-free problem in waves. Then a comparison is made among the values of the added resistance by the direct measurement using a dynamometer and by the wave-analysis method using the Fourier transform of measured and superposed waves. It is found that near the peak of the added resistance where ship motions become large, the degree of nonlinearity in the unsteady wave becomes prominent especially at the fore-front part of the wave. Thus the added resistance evaluated with measured waves at larger amplitude of incident wave becomes much smaller than the values by the direct measurement and by the wave analysis with superposed waves or measured waves at smaller amplitude of incident wave. Discussion is also made on the characteristics of the added resistance in the range of short incident waves.

2. Unsteady Wave Analysis and Added Resistance

We consider a ship advancing at constant forward speed U into a regular incident wave of amplitude A, circular frequency ω_0. The depth of water is assumed infinite; thus the wavenumber of incident wave is given by $k_0 = \omega_0^2/g$, with g the acceleration due to gravity. Corresponding to the experiment, only the head wave is considered, and the analysis is made with a right-handed Cartesian coordinate system O-xyz, with the origin placed at the center of a ship and on the undisturbed free surface, which translates with the same constant speed as that of a ship along the positive x-axis. The positive z-axis is taken upward. The unsteady responses of ship and associated ambient flow of fluid are assumed to be periodic with circular frequency of encounter $\omega = \omega_0 + k_0 U$.

By assuming the flow inviscid with irrotational motion, the velocity potential is introduced and written in the form

$$\boldsymbol{\Phi}(\boldsymbol{x},t) = U\big\{ -x + \phi_S(\boldsymbol{x})\big\} + \mathrm{Re}\Big[\big\{ \phi_0(\boldsymbol{x}) + \phi(\boldsymbol{x})\big\}\, e^{i\omega t}\Big]\,, \tag{1}$$

where $\boldsymbol{x} = (x, y, z)$ and $\phi_S(\boldsymbol{x})$ denotes the steady disturbance potential; $\phi_0(\boldsymbol{x})$ and $\phi(\boldsymbol{x})$ are the spatial part of the incident wave and unsteady disturbance potentials, respectively. By linear assumption, the disturbance potential $\phi(\boldsymbol{x})$ is decomposed as follows:

$$\phi(\boldsymbol{x}) = \frac{igA}{\omega_0}\varphi_7(\boldsymbol{x}) + \sum_{j=1,3,5} i\omega X_j \ell_j \varphi_j(\boldsymbol{x})\,. \tag{2}$$

Here $\varphi_7(\boldsymbol{x})$ denotes the scattering potential and $\varphi_j(\boldsymbol{x})$ the radiation potential due to the j-th mode of motion ($j = 1$, 3, 5 for surge, heave, and pitch, respectively) with X_j its complex amplitude. Symbol ℓ_j is adopted to express the length dimension for pitch; that is, $\ell_5 = L/2$ and $\ell_j = 1$ for surge and heave.

At a distance from a ship, the elevation of ship-generated unsteady wave may be computed by neglecting the contribution from the steady disturbance, in the form

$$\zeta(x,y) = -\frac{1}{g}\left(i\omega - U\frac{\partial}{\partial x}\right)\phi(x,y,0) \tag{3}$$

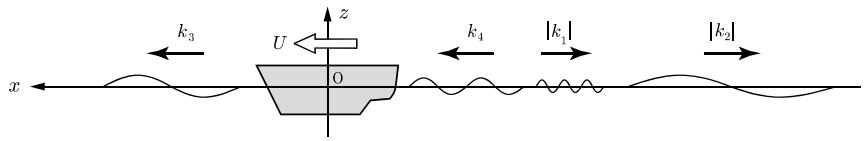

Fig. 1 Coordinate system and schematic illustration of wave components.

and each component of the unsteady disturbance potentials in (2) can be expressed by the far-field representation in the slender-ship theory as follows:

$$\varphi_j(x,y,0) = \int_L Q_j(\xi)\, G(x-\xi,y,0)\, d\xi\,, \tag{4}$$

where $Q_j(x)$ denotes the source strength along the x-axis and $G(x,y,z)$ is the Green function, equivalent to the velocity potential due to an oscillating and translating source with unit strength. By substituting Eq. (2) and Eq. (4) into Eq. (3) and neglecting the local wave term in the Green function, the elevation of progressive wave can be computed from

$$\zeta(x,y) = \frac{i}{2\pi}\left[-\int_{-\infty}^{k_1} + \int_{k_2}^{k_3} + \int_{k_4}^{\infty} \right] C(k) \frac{(\omega+kU)}{\omega_0} \frac{\kappa}{\sqrt{\kappa^2-k^2}}\, e^{-ikx - i\epsilon_k |y| \sqrt{\kappa^2-k^2}}\, dk\,, \tag{5}$$

where

$$\left.\begin{aligned} \kappa &= \frac{1}{g}\big(\omega+kU\big)^2 = K + 2k\tau + \frac{k^2}{K_0} \\ K &= \frac{\omega^2}{g},\ \tau = \frac{U\omega}{g},\ K_0 = \frac{g}{U^2},\ \epsilon_k = \operatorname{sgn}(\omega+kU) \end{aligned}\right\} \tag{6}$$

$$\left.\begin{matrix} k_1 \\ k_2 \end{matrix}\right\} = -\frac{K_0}{2}\big(1+2\tau \pm \sqrt{1+4\tau}\big)\,, \quad \left.\begin{matrix} k_3 \\ k_4 \end{matrix}\right\} = \frac{K_0}{2}\big(1-2\tau \mp \sqrt{1-4\tau}\big)\,, \tag{7}$$

$$C(k) = A\left[C_7(k) + \frac{\omega\omega_0}{g} \sum_{j=1,3,5} \frac{X_j \ell_j}{A} C_j(k) \right], \quad C_j(k) = \int_L Q_j(\xi)\, e^{ik\xi}\, d\xi\,. \tag{8}$$

Here $C_j(k)$ is known as the Kochin function (wave amplitude function) due to each component in the disturbance potential, and $C(k)$ in Eq. (8) is the total Kochin function for the motion-free case. The complex amplitude of the j-th mode of ship motion, $X_j\,(j=1,3,5)$, must be determined from the coupled motion equations.

In accordance with Eq. (8) for the Kochin function, the spatial part of ship-generated progressive wave $\zeta(x,y)$ can be written as the linear superposition of scattering wave $\zeta_7(x,y)$ and radiation waves $\zeta_j(x,y)$ by surge $(j=1)$, heave $(j=3)$, and pitch $(j=5)$ motions, in the form

$$\zeta(x,y) = A\left[\zeta_7(x,y) + \sum_{j=1,3,5} \frac{X_j \ell_j}{A} \zeta_j(x,y) \right]. \tag{9}$$

Noting that the wavenumbers k_j $(j=1\sim 4)$ appearing as the limits of integration in Eq. (5) are the roots of $\kappa^2 = k^2$ and $\epsilon_k = \operatorname{sgn}(\omega+kU) = -1$ for $-\infty < k < k_1$ and $\epsilon_k = 1$ for $k_2 < k < \infty$, we can write the elevation of progressive wave, Eq. (5), in the form

$$\zeta(x,y) = \frac{i}{2\pi} \int_{-\infty}^{\infty} u(\kappa^2-k^2)\, C(k) \sqrt{\frac{\kappa}{k_0}}\, \frac{\kappa}{\sqrt{\kappa^2-k^2}}\, e^{-ikx - i\epsilon_k |y| \sqrt{\kappa^2-k^2}}\, dk\,, \tag{10}$$

where $u(\kappa^2-k^2)$ is the unit step function, equal to 1 for $\kappa^2 > k^2$ and zero otherwise.

Let us consider the Fourier transform of $\zeta(x,y)$ with respect to x, defined by the following integral:

$$\zeta^*(\ell,y) = \int_{-\infty}^{\infty} \zeta(x,y)\, e^{i\ell x}\, dx\,. \tag{11}$$

Substituting Eq. (10) in Eq. (11) and using an integral representation of Dirac's delta function

$$\frac{1}{2\pi} \int_{-\infty}^{\infty} e^{i(\ell-k)x}\, dx = \delta(\ell-k)\,, \tag{12}$$

we can obtain with relative ease the following relation:

$$\zeta^*(k,y) = i\,C(k)\sqrt{\frac{\kappa}{k_0}}\frac{\kappa}{\sqrt{\kappa^2-k^2}}\,e^{-i\epsilon_k|y|\sqrt{\kappa^2-k^2}}\,. \tag{13}$$

According to Maruo's theory [1], the added resistance in head waves can be computed in terms of the Kochin function by the following formula:

$$R_{AW} = \frac{\rho g}{4\pi k_0}\left[-\int_{-\infty}^{k_1}+\int_{k_2}^{k_3}+\int_{k_4}^{\infty}\right]\big|\,C(k)\big|^2\,\frac{\kappa}{\sqrt{\kappa^2-k^2}}(k+k_0)\,dk\,. \tag{14}$$

Therefore, substituting Eq. (13) in Eq. (14) provides a formula for computing the added resistance with the Fourier transform of ship-generated unsteady waves, in the form

$$R_{AW} = \frac{\rho g}{4\pi}\left[-\int_{-\infty}^{k_1}+\int_{k_2}^{k_3}+\int_{k_4}^{\infty}\right]\big|\,\zeta^*(k,y)\big|^2\,\frac{\sqrt{\kappa^2-k^2}}{\kappa^2}(k+k_0)\,dk\,. \tag{15}$$

Here we should note a few things regarding the wavenumbers k_j $(j=1\sim4)$ appearing in Eq. (15). First, for $\tau>1/4$, k_3 and k_4 become complex as is obvious from Eq. (7), and the integration range in Eq. (15) must be treated as continuous for $k_2<k$. Next, $\omega=\omega_0+k_0U$ holds in head waves, which gives the following relations:

$$\left.\begin{aligned}\omega_0 &= \frac{g}{2U}\big(-1+\sqrt{1+4\tau}\big)\\ k_0 &= \frac{\omega_0^2}{g} = \frac{K_0}{2}\big(1+2\tau-\sqrt{1+4\tau}\big) = -k_2 = |k_2|\end{aligned}\right\} \tag{16}$$

On the other hand, it can be proven that the relation between the ship's speed U and the phase velocity c of a wave with wavenumber k_j $(j=1,3,4)$ along the x-axis is given by

$$\left.\begin{aligned}&0<U<\frac{c}{2} && \text{for } k_3\text{-wave}\\ &\frac{c}{2}<U<c && \text{for } k_4\text{-wave}\\ &c<U && \text{for } k_1\text{-wave}\end{aligned}\right\} \tag{17}$$

Since $c/2$ is equal to the group velocity with which the energy of progressive wave is transported, we can understand the location of existence, the relative wavelength, and the propagation direction when viewed from a ship moving at forward speed U for each of the k_j-waves $(j=1\sim4)$; these are schematically shown in Fig. 1. It is noteworthy that at $\tau=1/4$, k_3 becomes equal to k_4 and U becomes equal to the group velocity of progressive wave. For $\tau>1/4$, no wave exists ahead of the ship.

3. Experiments

3.1 Tested ship models

In order to see the effect of bluntness of the ship model, two modified Wigley models with different bluntness were used in the experiments: one is a blunt model with wider breadth $(L/B=5.0)$ and the other is a slender model with $L/B=6.67$. For convenience, these ship models are called 'blunt' and 'slender' modified Wigley models, respectively, in the present study. These modified Wigley models can be expressed mathematically as

(1) Blunt modified Wigley model:

$$\eta = (1-\zeta^2)(1-\xi^2)(1+0.6\xi^2+\xi^4)+\zeta^2(1-\zeta^8)(1-\xi^2)^4 \tag{18}$$

(2) Slender modified Wigley model:

$$\eta = (1-\zeta^2)(1-\xi^2)(1+0.2\xi^2)+\zeta^2(1-\zeta^8)(1-\xi^2)^4 \tag{19}$$

where $\xi=x/(L/2)$, $\eta=y/(B/2)$, and $\zeta=z/d$. The principal dimensions of these two models are shown in Table 1.

In order to see also the degree of contribution of each component wave $\zeta_j(x,y)$ defined in Eq. (9) in the linear superposition of ship-generated unsteady waves to the added resistance, the experiments were conducted for the cases of wave diffraction (where ship motions are completely fixed), forced oscillations in heave and pitch

Table 1 Principal dimensions of 'blunt' and 'slender' modified Wigley models.

Item	Blunt	Slender
Length L(m)	2.5	2.0
Breath B(m)	0.5	0.3
Draft d(m)	0.175	0.125
Displacement ∇ (m^3)	0.13877	0.04205
Water-plane area A_w (m^2)	1.005	0.416
Gyrational radius κ_{yy}/L	0.236	0.248
Center of gravity KG (m)	0.145	0.0846

(where incident waves are absent), and free response in waves (where surge, heave, and pitch are free to respond to waves). These experiments were implemented for the two modified Wigley models in the same way.

The lateral distance of a longitudinal line used for the wave measurement from the centerline of a ship (x-axis) was set equal to $y = B/2+$ 0.1 m. The Froude number was $Fn = 0.2$ in all measurements in the present study.

The incident waves were generated basically with target amplitude set equal to $A = 3.0$ cm for the blunt modified Wigley model and $A = 2.5$ cm for the slender modified Wigley model (because the model size is different as shown in Table 1). When the wave steepness $2A/\lambda$ becomes larger than 1/30, the target value of incident wave amplitude was determined to satisfy $2A/\lambda = 1/30$.

In the present study, it is important to see the validity of linear superposition in the unsteady wave and associated nonlinear effects on the added resistance. Thus all experiments in waves were performed for $A = 1.0$ cm as well. In the forced oscillation tests, the oscillation amplitude was set equal to $X_3 = 1.0$ cm for heave and $X_5 = 1.364$ deg for pitch to ensure satisfaction of the linear assumption in the wave generation.

4. Results and Discussion

4.1 Blunt modified Wigley model

Various results on the added resistance are shown in Fig. 2. The results of direct measurement by a dynamometer are shown with closed circle for $A = 3.0$ cm and open circle for $A = 1.0$ cm. Corresponding results obtained by the unsteady wave analysis using measured waves at $A = 3.0$ cm and $A = 1.0$ cm are shown with closed triangle and open triangle, respectively. In addition, computed results by EUT (Enhanced Unified Theory) are shown with solid line. We can see a large discrepancy between the results by the direct measurement and the unsteady wave analysis, particularly near the peak, but the results by the wave analysis at $A = 1.0$

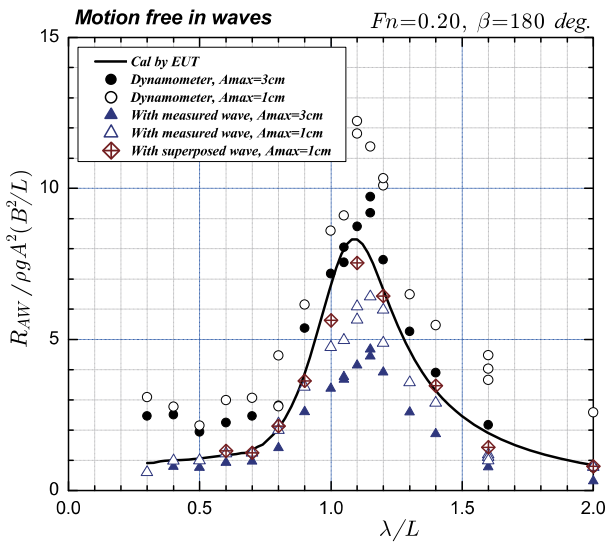

Fig. 2 Added resistance on the blunt modified Wigley model at $Fn = 0.2$ in the motion-free case.

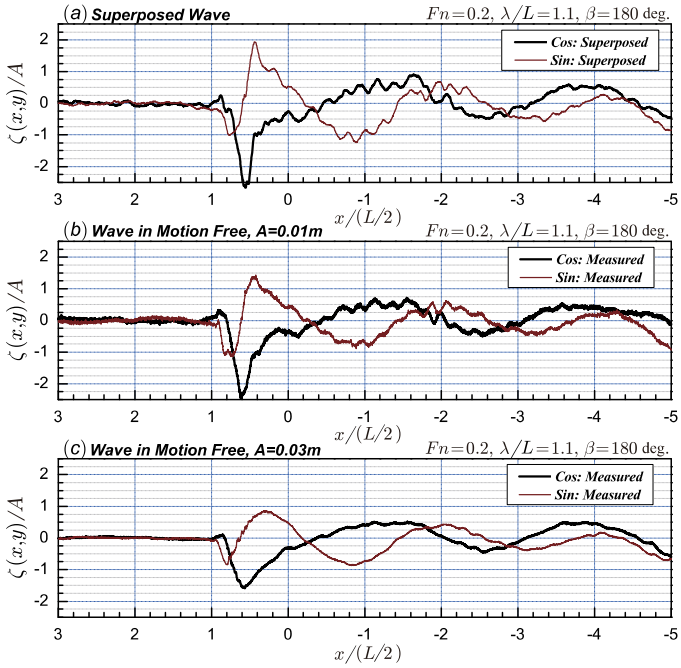

Fig. 3 Wave profiles generated by the blunt modified Wigley model at $Fn = 0.2$ in a regular wave of $\lambda/L = 1.1$. (a) Superposed wave, (b) Measured wave at $A = 1.0$ cm, (c) Measured wave at $A = 3.0$ cm.

cm are obviously larger than those by the wave analysis at $A = 3.0$ cm and approach the values of direct measurement and potential-flow computation by EUT.

In order to see and confirm the linearity in the unsteady wave, the wave profile was computed by the linear superposition according to Eq. (9), using the component waves obtained by the experiments of wave diffraction ($j = 7$), forced heave ($j = 3$), and forced pitch ($j = 5$), together with complex amplitudes of heave and pitch motions measured in the motion-free experiment. (The surge mode is not included, because the forced oscillation test in surge could not be conducted.) For the scattering wave and complex motion amplitudes in the linear superposition, the results measured at $A = 1.0$ cm are used. The superposed wave profile was Fourier-transformed and the added resistance was computed from Eq. (15). Obtained results from this linear superposition using component waves and complex amplitudes are also shown in Fig. 2 with diamond symbol. It is remarkable that these results are much closer to the results of direct measurement (especially at $A = 3.0$ cm) and computed ones by EUT. Furthermore, except near the peak, the results with superposed wave are very close to the ones with measured wave at $A = 1.0$ cm.

To see the difference at the level of wave profile, a comparison is shown among the superposed wave, measured wave at $A = 1.0$ cm and measured wave at $A = 3.0$ cm in Fig. 3 for $\lambda/L = 1.1$ as a typical example. From this comparison, we can see that the overall appearance of the wave profile is very similar between superposed and directly measured waves. However a prominent difference exists near the fore-front part of the wave; particularly in the wave measured at $A = 3.0$ cm, the fore-front part looks collapsed (or probably the wave breaking occurs) and the amplitude becomes small. At $\lambda/L = 1.1$, the superposed wave is still larger than the measured wave at $A = 1.0$ cm in the fore-front part and the component of short wavelength is more conspicuous; these differences are reflected in the results of the added resistance shown in Fig. 2.

The main source of difference in the fore-front part seems to come from the wave by the pitch motion. In order to show this fact visually, each wave profile of the component waves in the linear superposition is shown in Fig. 4 for the case of $\lambda/L = 1.1$ corresponding to the top figure in Fig. 3. From the top, (a), (b), and (c) are the scattering wave, heave radiation wave, and pitch radiation wave, respectively; these are normalized with unit amplitude. Furthermore, (d) and (e) are the heave and pitch component waves obtained after the measured

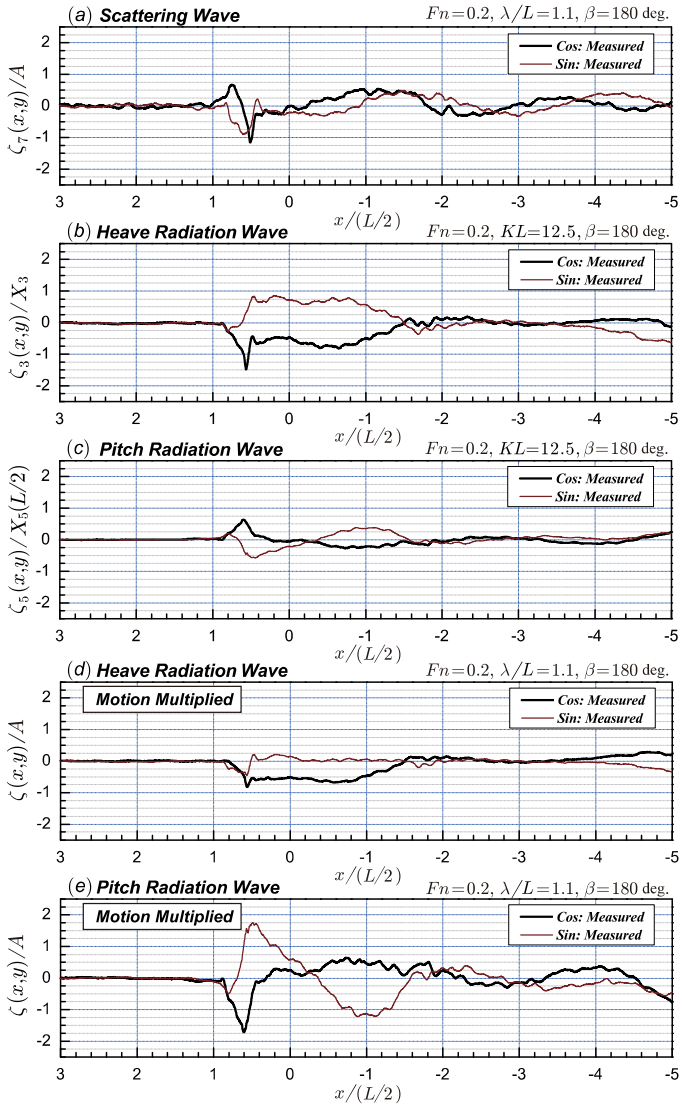

Fig. 4 Component waves in the linear superposition generated by the blunt modified Wigley model at $Fn = 0.2$ in a regular wave of $\lambda/L = 1.1$. (a) Scattering wave, (b) Heave radiation wave, (c) Pitch radiation wave, (d) Heave radiation wave with motion complex amplitude multiplied, (e) Pitch radiation wave with motion complex amplitude multiplied.

complex amplitude of each mode is multiplied. Therefore, the summation of (a), (d) and (e) provides the result of superposed wave shown as the top figure in Fig. 3. From these figures we can see that each component wave contributes to a large amplitude in the fore-front part but the most dominant component is the pitch radiation wave. We should note that the forced oscillation tests were performed with relatively small amplitude ($X_3 = 1.0$ cm and $X_5 = 1.36$ deg) within the range of linear theory being valid. Therefore, when the amplitude of ship motions becomes large, linearity in the amplitude of generated wave is violated particularly near the ship's bow or shoulder part due to large pitch motion. As a result, some nonlinear higher-order local waves with energy dissipation may be generated.

4.2 Slender modified Wigley model

The results of the added resistance for the slender modified Wigley model are shown in Fig. 5, where the results of direct measurement by a dynamometer are indicated with closed circle for $A = 2.5$ cm and open circle for $A = 1.0$ cm; the results by the unsteady wave analysis using measured waves are indicated with closed triangle for $A = 2.5$ cm and open triangle for $A = 1.0$ cm; the results obtained from superposed waves are indicated with diamond symbol. The linear superposition of unsteady wave has been made exactly in the same manner as that for the blunt modified Wigley model, using the scattering wave and heave and pitch motions measured at $A = 1.0$ cm and the radiation waves obtained by the forced heave ($X_3 = 1.0$ cm) and pitch ($X_5 = 1.364$ deg) oscillations. For reference, computed results by EUT are also shown by solid line.

We can see a prominent discrepancy in the results obtained by the unsteady wave analysis between at $A = 2.5$ cm and at $A = 1.0$ cm near the peak, which is the same tendency as that in the blunt modified Wigley model. The values of the added resistance obtained from superposed waves are further larger and almost the same as directly measured values and in good agreement with computed results by EUT (except for a slight shift in the peak wavelength).

To see the difference in the wave profile, an example is shown at $\lambda/L = 1.1$ in Fig. 6, for superposed wave, measured waves at $A = 1.0$ cm and $A = 2.5$ cm. Obviously the wave measured at $A = 2.5$ cm is different from the others in the profile especially near the fore-front part of the wave and in the magnitude of short-wavelength component. We can see also a difference in the amplitude of the fore-front part even between the superposed wave and measured wave at $A = 1.0$ cm. These differences in the wave profile are reflected in the result of the added resistance shown in Fig. 5. This fact implies that higher-order nonlinear waves or nonlinear interactions with steady disturbance may exist and ship-generated waves actually break when the ship motions are large.

The wave profile $\zeta(x, y)$ can be reproduced by the inverse Fourier transform with respect to k of the Fourier-transformed wave data $\zeta^*(k, y)$. In this computation, we can extract the wave in a specified wavenumber range (say, $\beta < k < \alpha$) from the following calculation:

$$\zeta_{\beta<k<\alpha}(x, y) = \frac{1}{2\pi} \int_{\beta}^{\alpha} \zeta^*(k, y)\, e^{-ikx}\, dk \tag{20}$$

In the present study, the superposed or measured wave is decomposed into the wave groups in the following

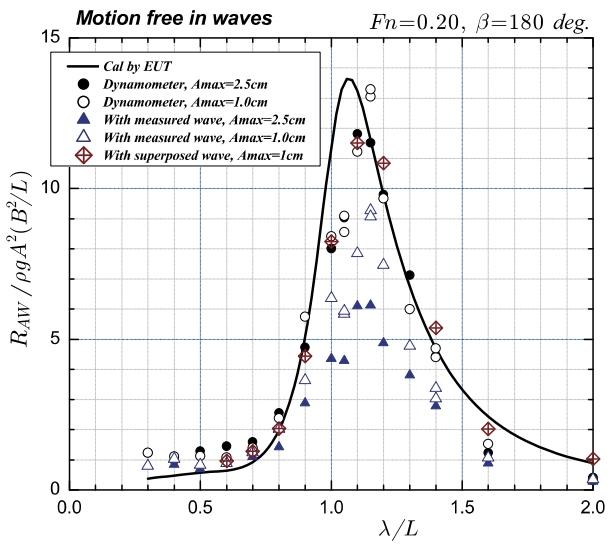

Fig. 5 Added resistance on the slender modified Wigley model at $Fn = 0.2$ in the motion-free case.

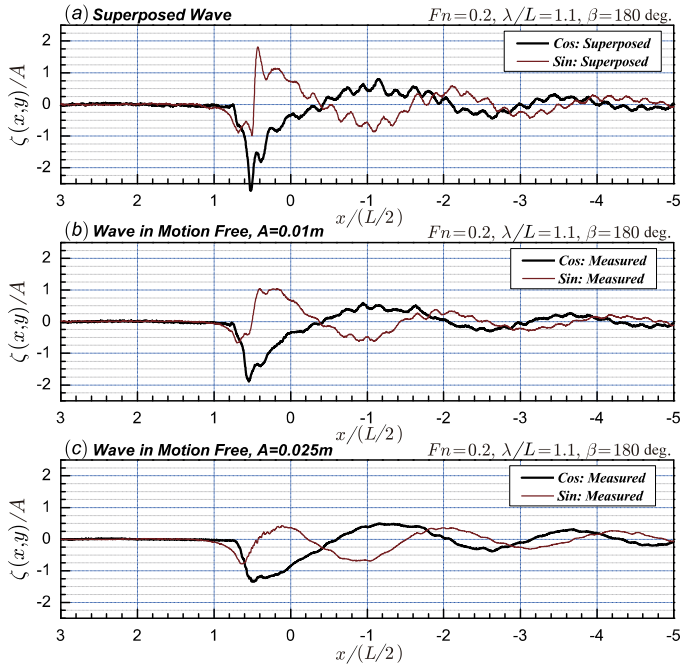

Fig. 6 Wave profiles generated by the slender modified Wigley model at $Fn = 0.2$ in a regular wave of $\lambda/L = 1.1$. (a) Superposed wave, (b) Measured wave at $A = 1.0$ cm, (c) Measured wave at $A = 2.5$ cm.

four different wavenumber ranges:

$$\left.\begin{array}{l} \text{Range-1}: \ -50 < k < k_1\,, \\ \text{Range-2}: \ k_1 < k < 0\,, \\ \text{Range-3}: \ 0 < k < k_C\,, \\ \text{Range-4}: \ k_C < k < 50 \end{array}\right\} \tag{21}$$

where $k_C = \omega/U = K_0\tau$ and k_1 is given by Eq. (7). It should be noted here that the wave groups in Range-1 and Range-4 have been neglected conventionally in computation of the added resistance (e.g. Ohkusu [2]) as short-wavelength components giving less contribution.

In the case of $\lambda/L = 1.1$ and slender modified Wigley model shown in Fig. 6, computed results from the superposed wave are shown in Fig. 7 and corresponding ones from the measured wave at $A = 2.5$ cm are shown in Fig. 8. It can be seen from Fig. 7 that the wave around the fore-front part includes various wave components and especially short-wavelength components are not necessarily small. On the contrary, Fig. 8 obtained from the measured wave at $A = 2.5$ cm tells us that short-wavelength components are very small even at the fore-front part and longer-wavelength components are almost the same as those in Fig. 7. These results suggest that a difference in prediction of the added resistance originates from relatively short wavelength components around the fore-front part and thus higher resolution for those wave components in the numerical computation is a key for enhancement in the prediction of the added resistance.

4.3 Added resistance at short incident waves

Up to the preceding subsection, attention has been focused on the difference near the peak of the added resistance. However, as seen in Fig. 2, directly measured results of added resistance on the blunt modified Wigley model in the short-wavelength region are obviously larger than those obtained from the unsteady wave analysis. In this region, the dominant component in the added resistance is due to wave diffraction, because wave-induced unsteady ship motions are generally negligible.

To see the magnitude and trend of the added resistance in the diffraction problem (where ship motions are completely fixed), the results of the added resistance in this case are plotted and compared in the same manner as in the motion-free case. Fig. 9 shows the result for the blunt modified Wigley model, and Fig. 10 shows

the corresponding result for the slender modified Wigley model. (The results at $A = 3.0$ cm for the blunt modified Wigley model were confirmed to be essentially the same as those obtained in the previous experiment, Kashiwagi *et al* [3].) From these figures we can see that: (1) the added resistance is almost constant irrespective of the incident-wave length, (2) the results obtained from the wave analysis are in acceptable agreement with computed values by EUT, and (3) directly measured values by a dynamometer are slightly larger than those by the wave analysis especially in the short-wavelength region.

More importantly, from a comparison with the results of motion-free case (specifically a comparison between Fig. 2 and Fig. 9), we can see that the added resistance in the motion-free case is obviously larger than that in the diffraction case at short incident waves; this tendency is prominent for the blunt modified Wigley model. In the range of short incident waves, although wave-induced motions are negligibly small, the steady sinkage and trim in the motion-free case are naturally nonzero. Because this is only the difference between the motion-free and diffraction cases in short incident waves, this difference can be a reason of the fact that the added resistance in the motion-free case is slightly larger than that in the diffraction case. This means that there must be interactions between steady and unsteady flows, and the effect of steady sinkage and trim should be taken into account in the prediction of the added resistance; which may become more important for blunt ships.

5. Conclusions

In order to study the contribution of unsteady wave-making component in the added resistance and nonlinear effects in ship-generated waves on the added resistance, experiments were conducted for measuring ship-generated unsteady waves, wave-induced ship motions, and the added resistance by using two different modified Wigley models and two different incident-wave amplitudes. The wave measurement was carried out for three canonical problems of wave diffraction with ship motions fixed, forced oscillations in heave and pitch, and free response of ship motions in waves. Then by using measured waves in the diffraction and radiation problems, the ship-generated unsteady wave was produced by the linear superposition.

Through comparisons of superposed waves with directly measured waves in the motion-free condition at

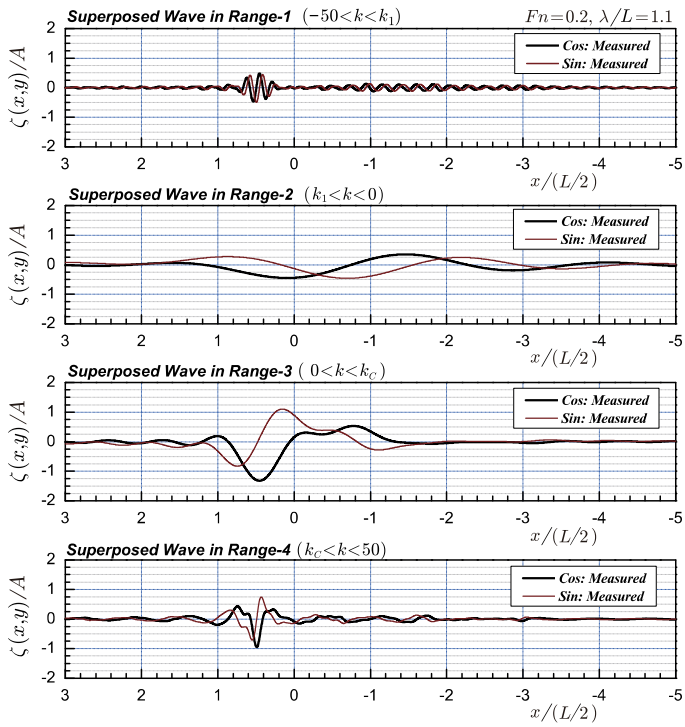

Fig. 7 Wave components extracted from superposed wave for the slender modified Wigley model at $Fn = 0.2$ and $\lambda/L = 1.1$.

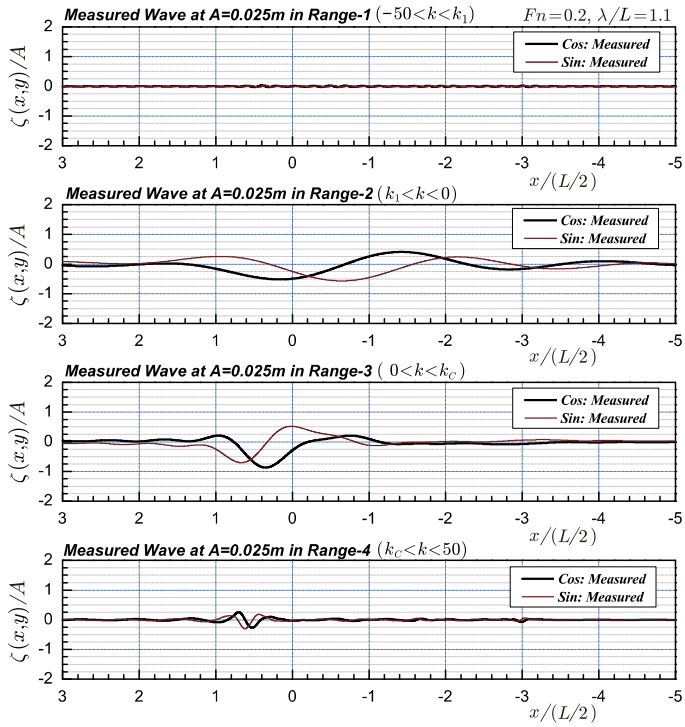

Fig. 8 Wave components extracted from measured wave for the slender modified Wigley model at $Fn = 0.2$ and in a regular wave of $\lambda/L = 1.1$ and $A = 2.5$ cm.

two different incident-wave amplitudes, nonlinearity in the wave elevation was studied and the effect of that nonlinearity on the added resistance has been investigated by means of the unsteady wave-analysis method. The results obtained in this study can be summarized as follows:

1) When ship motions become large near the peak of the added resistance, linearity in the unsteady wave elevation is not satisfied especially at the fore-front part of the wave. Consequently, the added resistance obtained from the waves measured at larger amplitude of incident wave becomes much smaller near the peak than those obtained from superposed linear waves and measured directly by a dynamometer.

2) The added resistance evaluated using superposed waves is in fairly good agreement with the result computed by the potential-flow theory (EUT in the present paper) over the range of wavelength tested.

3) The unsteady wave around the fore-front part consists of various wave components. In fact, short-wavelength components are not negligible in the linear waves and important in precise prediction of the wave profile at the fore-front part and hence of the added resistance.

4) At short incident waves, there was prominent difference in the added resistance on the blunt modified Wigley model between the values by the direct measurement and by the unsteady wave analysis. However, this difference is reduced in the diffraction problem where ship motions are completely fixed. This fact implies that the steady sinkage and trim should be taken into account in the prediction of the added resistance.

5) The added resistance in the diffraction problem is almost constant irrespective of the wavelength of incident wave, and the values of direct measurement by a dynamometer are almost the same as those obtained from the wave analysis. However, as the incident wave becomes short, directly measured values tend to be larger than the results of the wave analysis. This difference should be attributed to nonlinear effects which are not accounted for in the potential-flow theory.

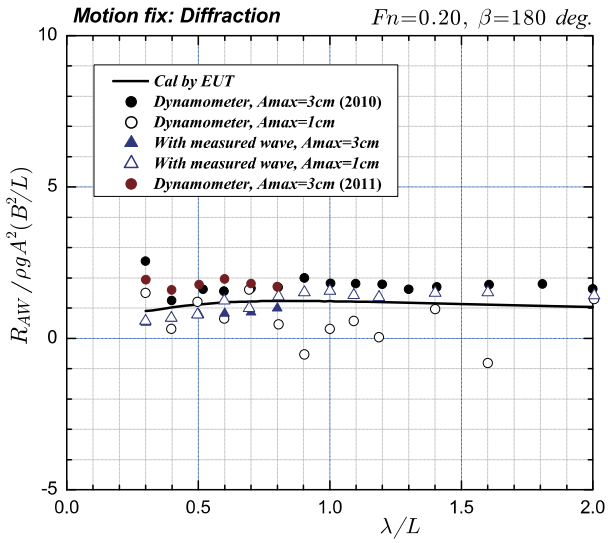

Fig. 9 Added resistance on the blunt modified Wigley model at $Fn = 0.2$ in the diffraction problem.

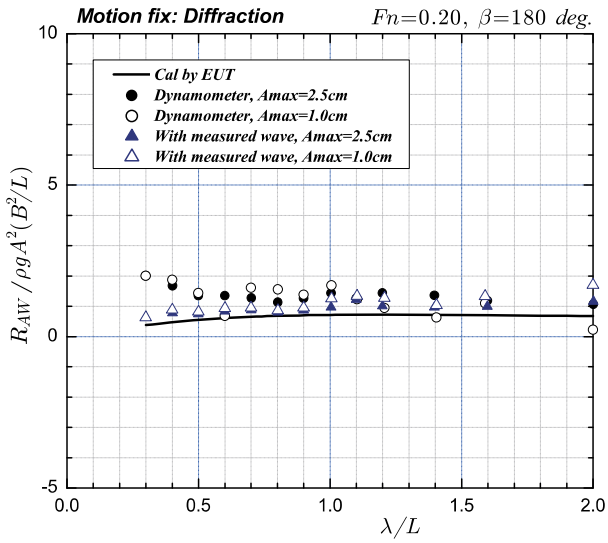

Fig. 10 Added resistance on the slender modified Wigley model at $Fn = 0.2$ in the diffraction problem.

References

1) Maruo, H (1960). "Wave resistance of a ship in regular head seas", *Bulletin of the Faculty of Engineering, Yokohama National University*, Vol 9, pp 73–91.

2) Ohkusu, M (1980). "Added Resistance in Waves in the Light of Unsteady Wave Pattern Analysis", *Proc of 13th Symposium on Naval Hydrodynamics*, Tokyo, pp 413–425.

3) Kashiwagi, M, Sasakawa, T and Wakabayashi, T (2011). "Hydrodynamic Consideration on Added Resistance and Ship-generated Unsteady Waves", *Proc 26th Intl Workshop on Water Waves and Floating Bodies*, Athens, pp 69–72.